# Magnonic control of the superconducting spin valve by magnetization reorientation in a helimagnet

Cite as: Appl. Phys. Lett. **118**, 232601 (2021); https://doi.org/10.1063/5.0055457
Submitted: 29 April 2021 . Accepted: 21 May 2021 . Published Online: 11 June 2021

N. A. Gusev, D. I. Dgheparov, N. G. Pugach, and V. I. Belotelov

Applied Physics Letters ARTICLE scitation.org/journal/apl

# Magnonic control of the superconducting spin valve by magnetization reorientation in a helimagnet

Cite as: Appl. Phys. Lett. **118**, 232601 (2021); doi: 10.1063/5.0055457
Submitted: 29 April 2021 · Accepted: 21 May 2021 ·
Published Online: 11 June 2021



N. A. Gusev,[1,2,a)] D. I. Dgheparov,[3] N. G. Pugach,[3,4] and V. I. Belotelov[1,2,4]

## AFFILIATIONS

[1]V.I. Vernadsky Crimean Federal University, Vernadsky Prospekt, 4, Simferopol 295007, Russia
[2]Russian Quantum Center, Bolshoy Bulvar 30 b.1, Moscow 121205, Russia
[3]HSE University, Moscow 101000, Russia
[4]Lomonosov Moscow State University, Leninskie Gory, 1 (2), GSP-2 Moscow 119991, Russia

[a)]**Author to whom correspondence should be addressed:** nagusew@gmail.com

## ABSTRACT

We propose a method to control a bilayer superconducting spin valve (SSV) which does not perturb its superconducting state and is suitable for energy saving cryogenic electronics. This SSV consists of a superconducting layer and a helimagnetic layer of B20 family compounds, namely, Nb and spiral antiferromagnet MnSi. Thanks to unique properties of MnSi—broken inversion symmetry and cubic crystal lattice—there are a few ground state magnetic configurations with different directions of the magnetic spiral, divided by a potential barrier. Superconductivity in such a bilayer is controlled by the reorientation of the spiral vector in the MnSi layer, which leads to a change in the critical temperature of the Nb layer due to the proximity effect. The switching is proposed to be carried out by a several hundred ps in duration magnetic field pulse of several kOe in magnitude. Such a pulse does not destroy the superconducting state of the Nb layer by itself but leads to the excitation of magnons in the MnSi layer, which triggers the reorientation process of the magnetic spiral. After the completion of this process, the Nb layer switches into a normal state. Inverse switching returns the spiral to the initial state, opening the valve and turning on the superconducting state. The system can be switched there and back by a magnetic field of opposite signs along one direction in the layers plane, which allows an easy control. The switching time is estimated as several nanoseconds, which coincides with the scales of the STT-MRAM recording time.



Superconducting spintronics is a subsection of spintronics studying spin transfer in the materials where the phenomenon of superconductivity occurs at temperatures below the critical one.[1] Combining superconductors (S), with ferromagnetic layers (F), one is able to create heterostructures, where superconducting spin-valve effect occurs. It exhibits in the change of the critical temperature of the superconducting layer at the magnetization reversal in the magnetic layer and based on the proximity effect.[2–11] The use of this effect allows building superconducting spintronic logic elements and memory cells.

The effect of spin wave processes on superconducting spintronics devices was mainly investigated for Josephson junctions.[12–14] It was shown that the processing spins, although they do not suppress dc Josephson current,[15] produce time-dependent Andreev bound states dynamics and induce the spin triplet superconducting correlations resulting in ac Josephson spin currents.[16–20]

The use of so-called helimagnetic material as an F-layer makes possible to simplify the superconducting spin valve to two layers.[21,22] However, in these experiments the helimagnetic Ho[21] or Er[22] layer must be heated to $T > T_c$ to return the valve in the initial state, which destroys superconductivity and significantly complicates the control of this electronic device.

In some materials with B20 structure, such as MnSi or FeGe a helicoid (spiral) magnetic order arises.[23,24] Previously, we have proposed the SSV based on spiral re-orientation in B20 magnet and calculated the change of the critical temperature in the S-layer when the orientation of the spiral vector in the F-layer has been rotated.[25,26] The change of $T_c$ appears as a result of competition of two mechanisms: space averaging of internal magnetic field over the coherence length and opening a channel of Cooper pairs drainage from the S-layer related to equal-spin triplet superconducting correlations. However,

only the side of the problem that relates to the phenomena of superconductivity was considered. Meanwhile, for the development of real logical elements based on SSVE, it is necessary to consider also the "magnetic" side of the problem. Therefore, the goal of this study is to find a way of the spiral SSV (SSSV) switching.

Let us consider a heterostructure S/F, where S is Nb and F is MnSi representing B20 magnet [Figs. 1(a) and 1(b)]. The B20 family spiral antiferromagnets have cubic crystal lattice with relative symmetry, which provides energy degeneracy of spiral directions in the ground state. The most effective superconducting switch is between the magnetic ground state with the spiral vector parallel to the S-layer and inclined at maximal angle to the layer plane.[25] These magnetic states are separated by a potential barrier that provides the selectivity of magnetic element switching. The negative constant of cubic anisotropy yields four equivalent spiral vector directions aligned along the cubic cell diagonals in the ground state, as it takes place for MnSi.[27] For the preferred configuration, it leads to the spiral vector having one orientation parallel to the plane of the S-layer film and three other orientations inclined to this plane. At the switch between the first and one of the rest, the effect of the magnetic spiral on the S-layer changes its critical temperature.[25] One may choose the final spiral state at the maximal angle about 70° to the film plane. (It is the angle between cubic diagonals.)

Let us assume that in the initial state the spiral vector $\mathbf{q_1}$ is parallel to the S-layer plane, which provides higher $T_c$ of the S-layer, and in the final state the spiral vector is $\mathbf{q_2}$ coinciding with the cubic lattice diagonal inclined to the S-layer plane (Fig. 1). To maximize the angle between the S-layer plane and $\mathbf{q_2}$, the MnSi crystal should be cut in a way that the plane of vectors $\mathbf{q_1}$ and $\mathbf{q_2}$ is perpendicular to the layer plane [XOY plane in Fig. 1(c)]. The magnetic field direction should be perpendicular to both vectors $\mathbf{q_1}$ and $\mathbf{q_2}$, i.e., be applied in the S-layer plane. In this case, the magnetic pulse excites the precession most effectively, launces spin wave process, leading to the switching between these two states. After the magnonic relaxation and re-orienting of the

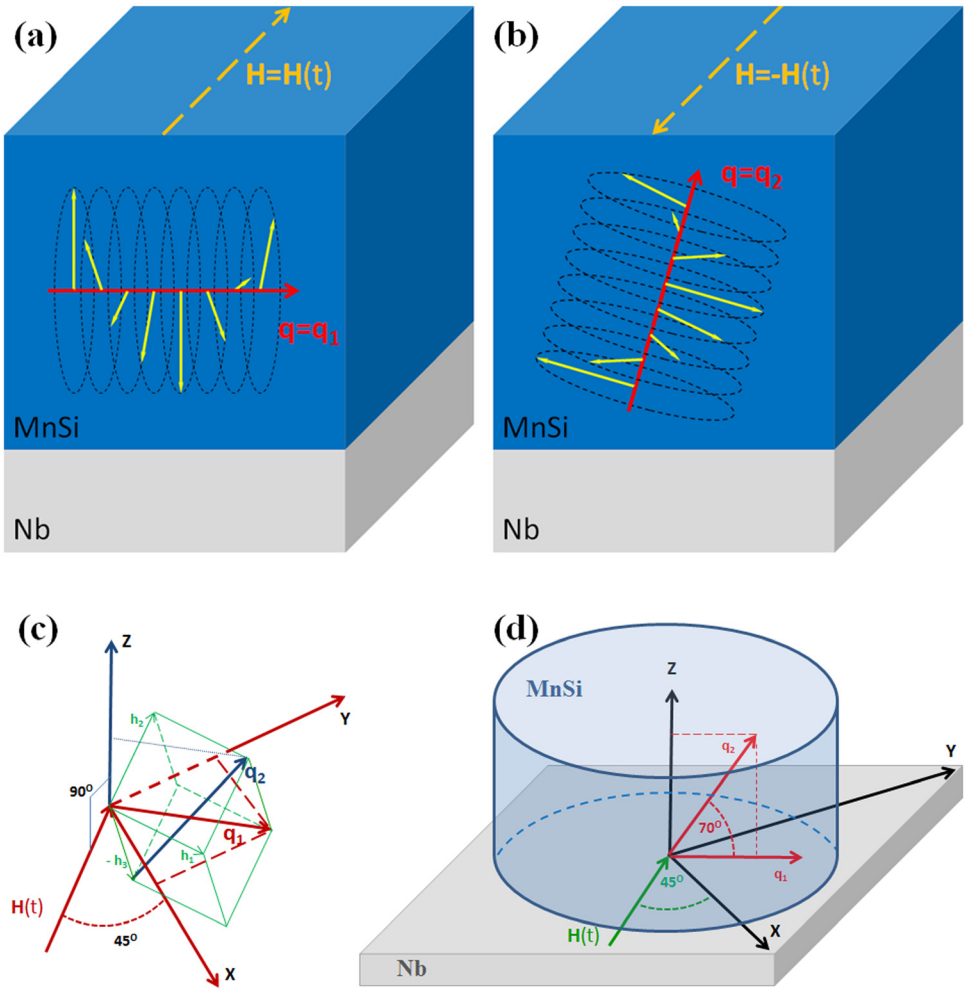


**FIG. 1.** (a) and (b) The concept of the SSV logic element. A superconducting (Nb) layer is deposited on a MnSi crystal. Initially, the spiral vector **q** of the F-layer is directed along $\mathbf{q_1}$ (a) and after applying a short magnetic field pulse **H**(t) the spin wave relaxation will turn it to the $\mathbf{q_2}$ direction (b). (c) Orientation of the cubic orthonormal anisotropy axes $\mathbf{h_1}$, $\mathbf{h_2}$, and $\mathbf{h_3}$ of the MnSi cylindrical sample relative to the coordinate system. (d) The cylindrical shape of the MnSi/Nb heterostructure.

magnetic spiral, the critical temperature of the S-layer vanishes, and the layer may become normal. One can realize the switch back to initial configuration by a similar magnonic process, starting by the pulse with magnetic field along the same direction but of different magnitude and sign, as we show further. Both processes are necessary to write the states "1" or "0" in the memory element based on the proposed SSV.

Typically, the spiral magnetic orientation can be easily changed by applying a sufficiently large magnetic field along the direction; the spiral vector is to be switched. The sample reaches magnetic saturation, and when the field is switched off, the magnetic configuration relaxes to the neighbor spiral ground state. However, this approach has several drawbacks, including appearance of the Abrikosov vortices and necessity to rotate an external magnetic field. It is much more advantageous to apply the switching field in a fixed direction parallel to the S-layer to avoid the Abrikosov vortices and to simplify the magnetic control of such memory elements.

Since the study is carried out by the solution of the Landau–Lifshitz–Gilbert equation, it is necessary to discuss the energy terms for the spiral magnet and the values of the parameters used for calculation of the energies. The free energy of a B20 lattice material with magnetization $\mathbf{M}$[28] is given by

$$E = A(gradM)^2 + D\mathbf{M}rot\mathbf{M} + (\mathbf{M}\cdot\mathbf{H}) + E_{ms} + E_{an}. \quad (1)$$

In Eq. (1), the first term corresponds to the Heisenberg exchange interaction, the second—to the bulk Dzyaloshinsky–Moriya interaction, and the third one—to the energy in an external field $\mathbf{H}$. Here $A$ is Heisenberg exchange constant, $D$ is the Dzyaloshinsky constant, and $\mathbf{M}$ is medium magnetization. The magnetostatic term $E_{ms}$ is determined by the shape and size of the film, and the anisotropic term, which is responsible for the spiral magnetic orientations, consists of the anisotropic exchange term, uniaxial and cubic magnetic anisotropy. Since we use bulk MnSi, the uniaxial anisotropy in our case is neglected. Anisotropic exchange interaction and cubic crystallographic anisotropy both lead to the same physical result, and usually in the experiment, it is hard to distinguish one from another. Therefore, all the anisotropy of the system may be considered as the cubic crystallographic anisotropy,

$$E_{an} = K_{cub}(M_x^2M_y^2 + M_x^2M_z^2 + M_y^2M_z^2) + inv(M), \quad (2)$$

where $K_{cub}$ is cubic anisotropy constant. The "inv" term indicates invariant about the modulus of magnetization, which is necessary to be added for normalization of the energy.

We used a cylinder with axis directed along the z-axis of the coordinate system as a shape of the MnSi. Such selection allows excluding the magnetic order distortion due to the anisotropy of the shape [Fig. 2(d)] similar to magnetic-tunnel-junctions MRAM cells. The cylinder diameter and thickness are 50 nm, which is more than twice the spiral order period $\lambda = 2\pi \times 2A/D \approx 18.5$ nm. The thickness of the S film must be about the critical one, allowed by the proximity with the magnet, of the order of 20 nm.[25] A sample size of about 5 coherence lengths is sufficient to change the critical temperature in the Nb layer after the spiral vector re-orientation. The cylinder thickness of 50 nm seems achievable at the current bulk MnSi fabrication and nanostructuration technique.[29] It meets the goal of electronics elements miniaturization. The small size of the sample and the absence of shape anisotropy allow ignoring the magnetostatic energy term in Eq. (1), e.g., $E_{ms}$= 0, which saves computational memory and greatly speeds up the calculation.

We rotate the MnSi crystal to put $\mathbf{q_1}$ in the layer plane XOY and $\mathbf{q_2}$ in the plane given by $\mathbf{q_1}$ and z-axis (see supplementary material). Such configuration greatly simplifies the geometry of the problem and allows one applying the magnetic field pulse in the XY plane for direct and inverse switching along direction of 135° or −45° to the X axis, respectively [Fig. 1(c)].

Thus, taking into account all simplifications, Eq. (1) takes the form

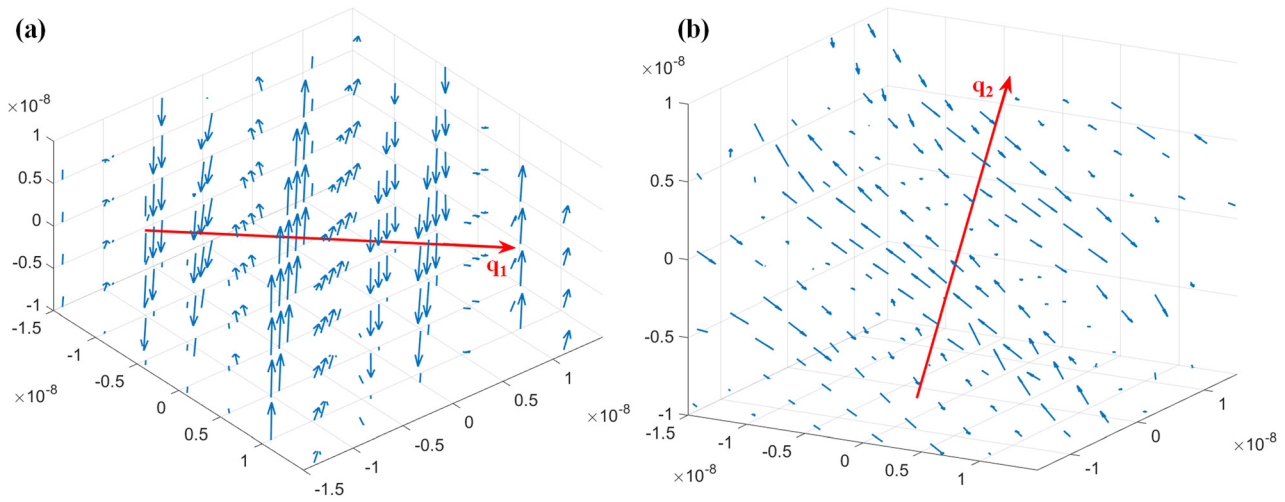


**FIG. 2.** The initial (a) and the final (b) states of the magnetization distribution in the MnSi layer. Short blue arrowed lines correspond to magnetic momentums and the red long arrowed line depicts the direction of the spiral vector. The axes are the x, y, and z coordinates in meters.

$$E = A(gradM)^2 + D\mathbf{M}rot\mathbf{M} + (\mathbf{M}\cdot\mathbf{H}) + K_{cub}\left(a_1^2a_2^2 + a_2^2a_3^2 + a_1^2a_3^2\right). \quad (3)$$

Here $a_1 = (\mathbf{m}\cdot\mathbf{h_1})$, $a_2 = (\mathbf{m}\cdot\mathbf{h_2})$, and $a_3 = (\mathbf{m}\cdot\mathbf{h_3})$, $\mathbf{m}$ is normalized magnetization and $\mathbf{h_1}$, $\mathbf{h_2}$, and $\mathbf{h_3}$ are the orthonormal anisotropy axes.

The applied magnetic field pulse $\mathbf{H}$ launching the magnonic process has a rectangular shape,

$$\mathbf{H}(t) = \begin{Bmatrix} \{-H_0/\sqrt{2}, H_0/\sqrt{2}, 0\},\ 0 \le t \le T \\ \{0,0,0\},\ t > T \end{Bmatrix}, \quad (4)$$

where $t$ is time, $H_0$ is the pulse amplitude, and $T$ is the pulse duration. The sign of $H_0$ should be reversed for the inverse switch. Minimization of the energy (3) yields the value of the effective field $H_{eff}$ and one can substitute it into the LLG equation. Integration of the LLG equation, taking into account the time-limited external magnetic affect, yields a picture of the spin waves propagation leading to the re-orientation of the spiral and the final state of spins in the spiral magnet. The simulation was carried out using the basic OOMMF package[30] with the additional module for bulk Dzyaloshinsky–Moriya interaction developed by David Cortés-Ortuño *et al.*[31] The Runge–Kutta method was used for the integration, and the computing cell was chosen as $1 \times 1 \times 1$ nm.

The realistic parameters for the simulations can be found from the experimental data for MnSi[32] by recalculation from the unit cell to the unit volume: $A = 36 \times 10^{-14}$ J/m, $D = 244 \times 10^{-6}$ J/m$^2$,[32,33] saturation magnetization $M_s = 163$ kA/m,[32] $K_{cub} = -51.2$ kJ/m$^3$,[34] the Gilbert damping constant $\alpha = 0.2$ (Supplementary).

Figure 2 demonstrates the distribution of the magnetization of the initial (a) and the final (b) states of the MnSi layer. They were obtained by relaxation from artificially iteration state via the energy minimization regime. The periodic structure of magnetization with a Bloch type structural element is clearly distinguishable: the magnetization rotates strictly around a certain direction, so that the spin projection on this direction is zero everywhere. This structure is known as a magnetic spiral, and the corresponding direction, the magnetization vector turns around, is a spiral vector. A spiral section located inside the sample corresponds approximately the two spiral periods. Imperfections of the spiral order associated with the limited sample size (boundary conditions) are observed at the sample edges. In the initial state [Fig. 2(a)], the vector of the spiral $\mathbf{q_1}$ located in the plane of the S film and has no projection onto the cylinder axis (the z-axis), and the distribution of magnetization along the z-axis is uniform. In the final state [Fig. 2(b)], the spiral is re-oriented in such a way that the spiral vector $\mathbf{q_2}$ acquires a nonzero projection onto the z-axis and the magnetization distribution becomes non-uniform along all three coordinate axes. In this case, the spiral vector makes an angle of approximately 70° with the film plane, and it should change the critical temperature in the S-layer deposited on the surface of the F-layer. The results presented in Fig. 2 confirm the correctness of the selected model and approximations.

Let us now simulate the magnonic propagation and relaxation process of the SSV switching and analyze its duration and resulting magnetic distributions. We consider application of magnetic field pulses up to 5.5 kOe in amplitude and 1000 ps in duration. Such values of the magnetic field are feasible[35] and cannot destroy the superconducting state of the Nb S-layer since its critical field is about several tens of kOe. The simulation results are presented by the switch table-like diagrams: the cells, indicated by green color correspond to the transition of the sample from the initial state $\mathbf{q_1}$ to the final one $\mathbf{q_2}$ for the case of direct switch [Fig. 3(a)], and from the final state to the initial one for the case of inverse switch [Fig. 3(b)]. For direct switch, the optimal magnetic field pulse was found to lie in the range 2300–3500 Oe of magnitude and 430–700 ps of duration. The switch was detected by visual coincidence of the distribution obtained during the simulation with the picture in Fig. 2(b). For the inverse switch, the sign inversed magnetic pulse of 3200–3800 Oe of magnitude and 218–299 ps of duration is optimal. Such a pulse being applied to the distribution $\mathbf{q_2}$ in Fig. 2(b) turns it to the state $\mathbf{q_1}$ which is compared with the distribution in Fig. 2(a). The unfilled cells (Fig. 3) correspond to the cases, when the system, in spite of the impact, returned to the initial state. Some intermediate states were also obtained, which did not coincide neither with the first ground state distribution nor with the second one. They are also marked by unfilled cells. The average simulation time was approximately 3.7 ns for the direct and 5.5 ns for the inverse switch, which makes one possible to estimate the switching frequency of the element as about 0.2 GHz. This time describes the duration of the magnonic relaxation initiated by the pulse and leading to the desired stable state. It corresponds to the operation time scales of the modern STT-MRAM.[36]

In the narrow intervals of magnitudes and durations of external magnetic field presented in bigger tables in Fig. 3, the system switches stably: for direct and for inverse switch, the system's response to the influence is identical at any points inside the green region (or unfilled one if only unswitched cases are considered), with the resolution of the (a) diagram as $9 \times 11$ and (b) diagram as $11 \times 10$ cells. In the wider ranges, which are presented in the smaller tables, the stability gradually disappears—the green or unfilled regions become not simply connected, but this phenomenon vanishes if the damping of the system (Gilbert parameter) is raised above 0.2.

The presented narrow green areas correspond to the optimal parameters of the external magnetic pulse (minimal magnitude at minimal duration) for the direct and inverse switch of the spiral states providing stability in the specified range (Fig. 3). Choosing $H_0 = 3050$ Oe and $t = 610$ ps for direct switch and $H_0 = 3530$ Oe and $t = 263$ ps for inverse one as the operative parameters of external field generator one can verify that stable switching is maintained even if these parameters fluctuate within 7.5%–10% of magnitude, which is easily achievable for modern electronics. The difference of the optimal pulse parameters for direct and inverse switch is due to the fact that configuration of the spiral vector $\mathbf{q_1}$, lying in the XY plane, corresponds to a higher symmetry, than the inclined configuration $\mathbf{q_2}$. The MnSi sample has the round shape in the XY plane, while the cross section of the sample by the plane, in which $\mathbf{q_2}$ lies, is square shaped. However, the parameters of the magnetic field pulse required for direct and inverse switch do not differ significantly and are achievable for the same hardware configuration, and the direction of the magnetic field can be changed simply by changing the direction of the current in the coil. The difference in the optimal field pulse parameters for the direct and inverse switching relates to the different position of the spiral vector in the cylindric sample.

We propose a method of effective control of the superconducting spin valve based on a spiral magnet of B20 family via a magnonic relaxation. Such spiral magnets have cubic crystal lattice, with few

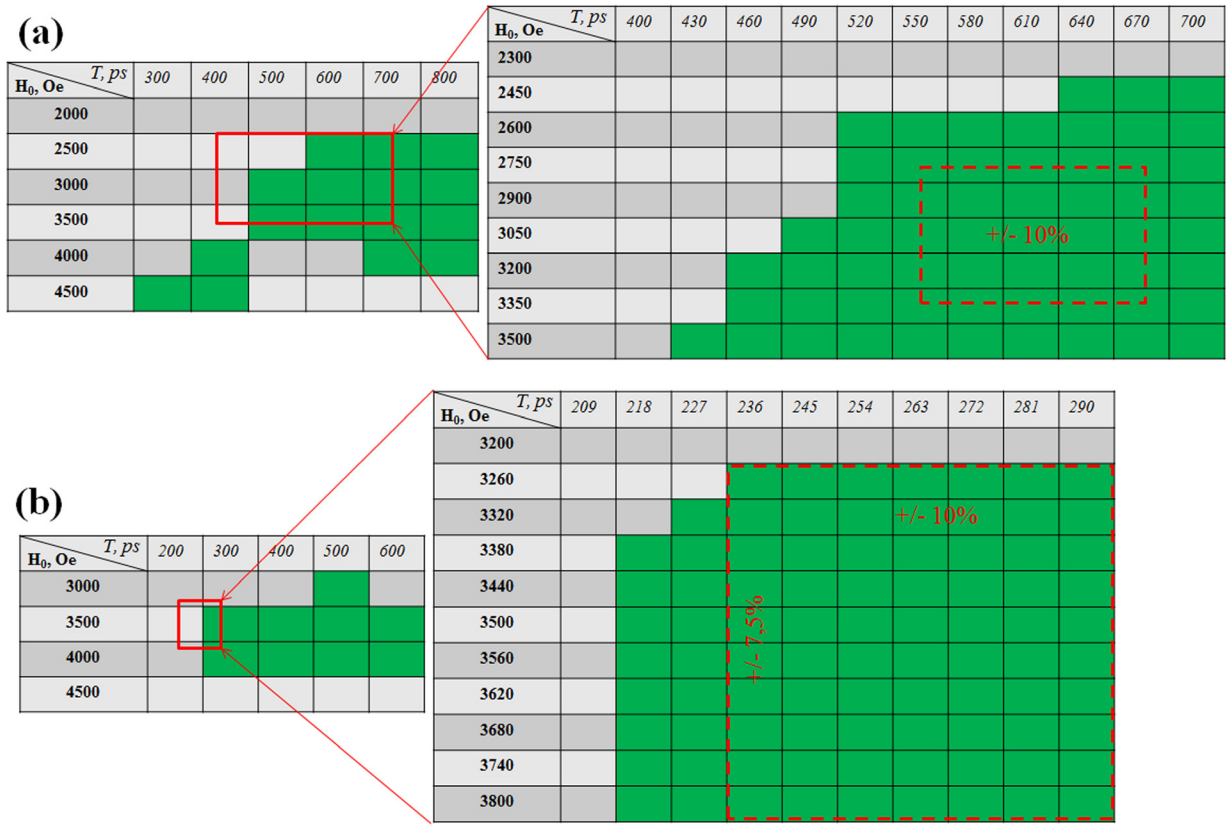


**FIG. 3.** Switching table diagrams for (a) direct and (b) inverse switching. A green cell corresponds to the switched state, and unfilled one corresponds to the intermediate state or returning the system to the primary state. The smaller tables correspond to the wider intervals of the parameters, and the bigger ones correspond to the shorter range.

preferred directions of the magnetic spiral divided by a potential barrier. It was shown that the reversable switch of the spiral direction between such two states with different angle to a thin superconducting film covered the magnetic sample, changes its critical temperature. It is the mechanism of the spiral SSV control. Numerical experiments were performed assuming MnSi as a spiral magnet covered by Nb film of the suitable thickness of about 20–30 nm, using realistic parameters taken from literature. It is shown that at the taken parameters the working point may be chosen as 3050 Oe, 610 ps for direct switch and 3500 Oe, 254 ps for the inverse one.

The proposed method has several important advantages. First of all, it solves the so-called half-select problem of the control of superconducting RAM:[35] the pulse of half-amplitude does not switch the SSV. The pulse magnetic field does not affect significantly the superconducting state of the film by itself. Moreover, both pulses for the direct and inverse switching lie in the film plane and should not affect the Abrikosov vortices. The magnetic field for direct and inverse switch lies along the same line that significantly simplified the control making possible record-readout via Savchenko scheme developed for MRAM. The method is stable in the range of 7%–10% of magnitude of the pulse parameters. The equilibration time may be estimated as about 5 ns that allows recording with the frequency about 0.2 GHz. The magnetic pulse itself is much shorter. The recording frequency is comparable with the frequency of modern MRAM, and the readout may be much faster. The SSV allows miniaturization of the memory element up to values about 20 nm limited by the spiral length or the S-layer coherence length. The scaling is restricted by the modern nanotechnology possibilities. Finally, the stored information conserves even at a heating above the superconducting $T_c$ up to the magnetic Neel temperature (29 K for MnSi).

All these make the considered method suitable for use in MRAM control scheme for magnetic memory in superconducting digital and quantum electronic devices. The control of a superconducting spintronic device via a spin-valve relaxation process started by a pulse magnetic field opens a way of magnonic control for superconducting memory merging quantum magnonics and superconducting electronics.

See the supplementary material for information about cubic anisotropy constant calculation, cubic anisotropy axes rotation matrix, and the Gilbert dumping parameter selection.

This work was financially supported by the Ministry of Science and Higher Education of the Russian Federation, Megagrant Project No. 075-15-2019-1934.

## DATA AVAILABILITY

The data that support the findings of this study are available from the corresponding author upon reasonable request.

## REFERENCES


[1]V. N. Kushnir, A. Sidorenko, L. R. Tagirov, and M. Y. Kupriyanov, *Functional Nanostructures and Metamaterials for Superconducting Spintronics* (Springer, Cham, 2018), p. 1.
[2]P. G. De Gennes, Phys. Lett. **23**(1), 10 (1966).
[3]S. Oh, D. Youm, and M. R. Beasley, Appl. Phys. Lett. **71**, 2376 (1997).
[4]Y. V. Fominov, A. A. Golubov, T. Y. Karminskaya, M. Y. Kupriyanov, R. G. Deminov, and L. R. Tagirov, JETP Lett. **91**(6), 308 (2010).
[5]R. R. Gaifullin, V. N. Kushnir, R. G. Deminov, L. R. Tagirov, M. Y. Kupriyanov, and A. A. Golubov, Phys. Solid State **61**(9), 1535 (2019).
[6]L. R. Tagirov, "Low-field superconducting spin switch based on a superconductor/ferromagnet multilayer," Phys. Rev. Lett. **83**(10), 2058 (1999).
[7]A. I. Buzdin, A. V. Vedyayev, and N. V. Ryzhanova, Europhys. Lett. **48**(6), 686 (1999).
[8]A. Vedyayev, C. Lacroix, N. Pugach, and N. Ryzhanova, Europhys. Lett. **71**(4), 679 (2005).
[9]A. V. Vedyayev, N. V. Ryzhanova, and N. G. Pugach, J. Magn. Magn. Mater. **305**, 53 (2006).
[10]G. Deutscher and F. Meunier, Phys. Rev. Lett. **22**(9), 395 (1969).
[11]J. J. Hauser, Phys. Rev. Lett. **23**(7), 374 (1969).
[12]A. F. Volkov and K. B. Efetov, Phys. Rev. Lett. **103**(3), 037003 (2009).
[13]S. Mai, E. Kandelaki, A. F. Volkov, and K. B. Efetov, Phys. Rev. B **84**(14), 144519 (2011).
[14]I. Petković, M. Aprili, S. E. Barnes, F. Beuneu, and S. Maekawa, Phys. Rev. B **80**(22), 220502 (2009).
[15]J. X. Zhu and A. V. Balatsky, Phys. Rev. B **67**(17), 174505 (2003).
[16]C. Holmqvist, S. Teber, and M. Fogelström, Phys. Rev. B **83**(10), 104521 (2011).
[17]M. Houzet, Phys. Rev. Lett. **101**(5), 057009 (2008).
[18]C. Richard, M. Houzet, and J. S. Meyer, Phys. Rev. Lett. **109**(5), 057002 (2012).
[19]J. P. Morten, A. Brataas, G. E. Bauer, W. Belzig, and Y. Tserkovnyak, Europhys. Lett. **84**(5), 57008 (2008).
[20]K. Rogdakis, A. Sud, M. Amado, C. M. Lee, L. McKenzie-Sell, K. R. Jeon, M. Cubukcu, M. G. Blamire, J. W. A. Robinson, L. F. Cohen, and H. Kurebayashi, Phys. Rev. Mater. **3**(1), 014406 (2019).
[21]A. D. Bernardo, S. Diesch, Y. Gu, J. Linder, G. Divitini, C. Ducati, E. Scheer, M. G. Blamire, and J. W. A. Robinson, Nat. Commun. **6**(1), 8053 (2015).
[22]N. Satchell, J. D. S. Witt, M. G. Flokstra, S. L. Lee, J. F. K. Cooper, C. J. Kinane, S. Langridge, and G. Burnell, Phys. Rev. Appl. **7**(4), 044031 (2017).
[23]V. A. Dyadkin, S. V. Grigoriev, D. Menzel, E. V. Moskvin, S. V. Maleyev, and H. Eckerlebe, Physica B **406**(12), 2385 (2011).
[24]B. Lebech, J. Bernhard, and T. Freltoft, J. Phys.: Condens. Matter **1**(35), 6105 (1989).
[25]N. G. Pugach, M. Safonchik, T. Champel, M. E. Zhitomirsky, E. Lähderanta, M. Eschrig, and C. Lacroix, Appl. Phys. Lett. **111**(16), 162601 (2017).
[26]N. G. Pugach and M. O. Safonchik, JETP Lett. **107**(5), 302 (2018).
[27]S. V. Grigoriev, S. V. Maleyev, S. I. Okorokov, Y. O. Chetverikov, and H. Eckerlebe, Phys. Rev. B **73**(22), 224440 (2006).
[28]P. Bak and M. H. Jensen, J. Phys. C **13**(31), L881 (1980).
[29]A. Tonomura, X. Yu, K. Yanagisawa, T. Matsuda, Y. Onose, N. Kanazawa, H. S. Park, and Y. Tokura, Nano Lett. **12**(3), 1673 (2012).
[30]M. J. Donahue and D. Porter, see http://math.nist.gov/oommf for "OOMMF (NIST)"
[31]D. Cortés-Ortuño6, M. Beg, V. Nehruji, L. Breth, R. Pepper, T. Kluyver, G. Downing, T. Hesjedal, P. Hatton, T. Lancaster, R. Hertel, O. Hovorka, and H. Fangohr, New J. Phys. **20**(11), 113015 (2018).
[32]E. A. Karhu, U. K. Rößler, A. N. Bogdanov, S. Kahwaji, B. J. Kirby, H. Fritzsche, M. D. Robertson, C. F. Majkrzak, and T. L. Monchesky, Phys. Rev. B **85**(9), 094429 (2012).
[33]J. Iwasaki, M. Mochizuki, and N. Nagaosa, Nat. Commun. **4**(1), 1463 (2013).
[34]M. Janoschek, M. Garst, A. Bauer, P. Krautscheid, R. Georgii, P. Böni, and C. Pfleiderer, Phys. Rev. B **87**(13), 134407 (2013).
[35]I. V. Vernik, V. V. Bol'ginov, S. V. Bakurskiy, A. A. Golubov, M. Y. Kupriyanov, V. V. Ryazanov, and O. A. Mukhanov, IEEE Trans. Appl. Supercond. **23**(3), 1701208 (2013).
[36]C. Bi, N. Sato, and S. X. Wang, *Advances in Non-Volatile Memory and Storage Technology* (Woodhead Publishing, 2019), Vol. 203.